Nucleation mechanisms of self-induced GaN nanowires grown on an amorphous interlayer

V. Consonni,* M. Hanke, M. Knelangen, L. Geelhaar, A. Trampert, and H. Riechert
Paul-Drude-Institute for Solid State Electronics, Hausvogteiplatz 5–7, D-10117 Berlin, Germany
(Received 10 September 2010; revised manuscript received 16 November 2010; published 18 January 2011)

The formation mechanisms of GaN nanowires grown on a Si_xN_y amorphous interlayer within a self-induced approach by molecular beam epitaxy have been investigated by combining *in situ* reflection high-energy electron-diffraction measurements with *ex situ* high-resolution transmission electron microscopy imaging. It is found that GaN initially nucleates as spherical cap-shaped islands with a wetting angle of $42 \pm 7^\circ$. Subsequently, these islands coarsen and undergo a shape transition toward the nanowire morphology at an experimental critical radius of 5 nm. As the epitaxial constraint is very weak on an amorphous interlayer, the equivalent Laplace pressure due to the effects of surface stress has been taken into account. Analytical and finite-element method calculations show that the Laplace pressure results at the nanoscale dimensions in significant volume elastic strain in both spherical caps and nanowires. From thermodynamic considerations, it is revealed that the related strain energy density is slightly in favor of the shape transition toward the nanowire geometry owing to its higher ability to relieve the strain. Nevertheless, the anisotropy of surface energy is an even stronger driving force, since the nanowires are composed of *c*- and *m*-planes with very low surface energies. It is deduced that an energy barrier does exit for the shape transition and may be related to edge effects, resulting in a growth condition-dependent critical radius.

DOI: 10.1103/PhysRevB.83.035310 PACS number(s): 81.15.Hi, 62.23.Hj, 81.05.Ea

I. INTRODUCTION

The growth of semiconductor nanowires (NWs) paves the way to the fabrication of new three-dimensional nanostructures without the use of any advanced lithography. Their high aspect ratio in the nanoscale dimensions and their compatibility with silicon-based technology are very promising for a wide variety of chemical, electrical, and optical nanodevices.[1,2] Until now, the popular vapor-liquid-solid mechanism has generally been carried out to grow silicon, germanium, III-V arsenide, and phosphide NWs.[3–6] Still, some compound semiconductors with a wurtzite type crystalline structure such as nitrides and zinc oxide have recently received increasing interest due to their ability to spontaneously grow as NWs within a self-induced approach (i.e., catalyst-free) by molecular beam epitaxy (MBE) or chemical vapor deposition (CVD) for instance.[7–10] The self-induced growth is a promising alternative approach since it avoids the use of any foreign material and any substrate prepatterning, hence limiting the NW contamination and the resulting deterioration of their optical and structural quality.[11] Nevertheless, in contrast to the catalyst-induced growth, the main physical processes governing the nucleation and growth phases within this approach are still open. The surface diffusion of adatoms on the substrate and along the NW vertical sidewalls can account for the NW lengthening during the growth phase once NW nuclei have been formed,[12–14] but very little is known concerning the nucleation mechanisms leading to the self-induced formation of these very first NWs.[15]

It has recently been shown that the nucleation mechanisms of GaN NWs epitaxially grown by plasma-assisted MBE on a crystalline AlN buffer layer are deeply related to the relaxation process of the lattice-mismatch-induced (i.e., epitaxial) strain.[16–18] An initial process of elastic relaxation proceeds through several successive shape transitions and is followed by a complete plastic relaxation within full pyramids, which results in the formation of the very first NWs.[16,17] This nucleation mechanism can account for the self-induced formation of epitaxial nitrides NWs, for which a strong epitaxial relation with the substrate operates. However, it is well known that GaN NWs can also be grown by plasma-assisted MBE on a thin amorphous layer like silicon dioxide or silicon nitride.[19,20] If self-induced GaN NWs are directly grown on silicon without an AlN buffer layer, such an amorphous interlayer inevitably forms owing to the use of an active nitrogen flux leading to a nitridation process.[21] In this case, the previous relaxation process cannot be involved since it is expected that the epitaxial relation with the substrate is much weaker. It has been suggested that GaN clusters are formed in the very early stages of the nucleation process and could act as a seed for the self-induced formation of NWs.[19] Cheze *et al.* have also pointed out the interplay between the processes of silicon substrate nitridation and NW self-induced formation but the exact nucleation mechanism is still an open question.[21]

In this article, the aim is to experimentally investigate these nucleation mechanisms occurring during the self-induced formation of GaN NWs on an amorphous interlayer by combining *in situ* reflection high-energy electron diffraction (RHEED) measurements with high-resolution transmission electron microscopy (HRTEM) imaging. As the strain induced by the lattice mismatch is unlikely to play a role in this case, the effects of surface stress that is expected to induce some significant volume elastic strain at the nanoscale dimensions are taken into account by finite-element method (FEM) calculations and modeled within the approach given by Cammarata *et al.*[22] From analytical calculations, the role of the anisotropy of surface free energy as a major driving force and of the effects of edge energy as an energy barrier is revealed through thermodynamic considerations.

II. EXPERIMENT

All the samples were grown on Si(111) substrates by radio-frequency plasma-assisted MBE. The active nitrogen

species and gallium atoms were supplied by a plasma source operating at 500 W power with a 2-sccm flux and by a thermal effusion cell, respectively. Prior to GaN NW growth, a Si_xN_y amorphous interlayer was initially formed: the Si(111) substrate was exposed for 5 min to an active nitrogen flux to induce a nitridation process. GaN NWs were subsequently grown at a high substrate temperature of 780°C under highly nitrogen-rich conditions with a V/III ratio of 6.2. *In situ* reflection high-energy electron diffraction (RHEED) measurements were carried out during the entire growth process using an electron gun operating with a 2A filament current and 20 kV acceleration voltage. The incident-beam angle with the sample was 3°. One RHEED pattern was recorded every 12 s: The RHEED intensity was determined by monitoring *in situ* the diffraction intensity in a fixed rectangular area at a given position that involves several GaN 3D spots, as depicted by the dashed white rectangle in the inset of Fig. 1.[16,17] The evolution of the GaN spot intensity was then assessed by integrating and summing the overall area over each GaN 3D spot: it should be noted that the background intensity between each GaN 3D spot corresponding to the diffusive contribution was not taken into account. In order to combine the RHEED measurements with a microstructural analysis, cross-sectional TEM specimens were prepared from dedicated samples grown at different durations of 7, 11, 16, and 24 min, including the incubation time, by mechanical lapping and polishing followed by argon ion milling according to standard techniques. The incubation time corresponds to the initial period once both the gallium and nitrogen shutters are open during which no RHEED signal is detected: Its meaning is discussed later. HRTEM experiments were performed with a JEOL 3010 microscope operating at 300 kV.

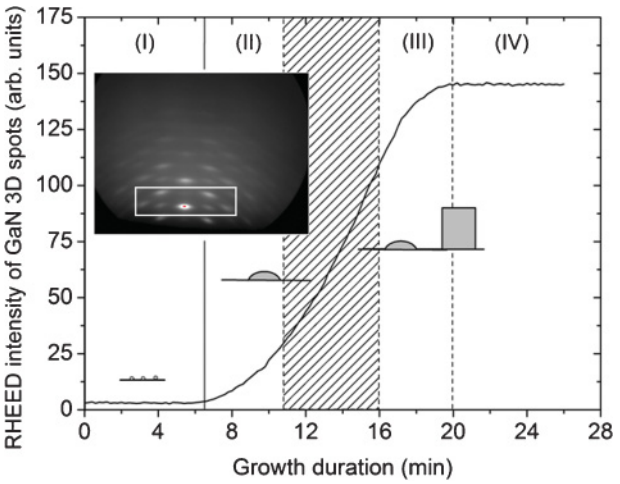

FIG. 1. Evolution of the RHEED intensity as growth proceeds. Four distinct consecutive regions are distinguished within such an analysis. The first insets represent simple sketches of GaN island shape, as observed by HRTEM images in Fig. 2 recorded on dedicated samples. The dashed zone points out that the first spherical cap undergoing a shape transition toward the NW morphology takes place between a growth duration of 11 and 16 min according to HRTEM imaging. The second inset represents a typical RHEED pattern of the GaN NWs (40 min). The rectangular area depicted by dashed white lines yields the RHEED intensity from the GaN 3D spots.

The analytical calculations have been carried out within the approach given by Cammarata *et al.* in order to determine the equivalent Laplace pressure acting on the island surfaces due to the effects of surface stress.[22] The FEM calculations have subsequently been performed with the commercial MarcMentat program package by implementing the equivalent Laplace pressure determined from the analytical calculations. The geometrical parameters, such as, in particular, the island shape, can be freely chosen. Thus, the model can accordingly be created in correlation with the experimental observations from HRTEM imaging. There are only a few further input parameters to implement, namely the elastic constants c_{ij} of wurtzite GaN [$c_{11} = c_{22} = 390$ GPa, $c_{12} = 145$ GPa, $c_{13} = c_{23} = 106$ GPa, $c_{33} = 398$ GPa, $c_{44} = c_{55} = 105$ GPa, $c_{66} = 0.5(c_{11} - c_{12})$] and the fixed mechanical boundary condition.[23]

III. RESULTS AND DISCUSSION

A. Nucleation process at the very early stages of self-induced NW growth

The evolution of the RHEED intensity is presented in Fig. 1 and reveals in correlation with the HRTEM images that the nucleation process consists of four consecutive different stages. Typically, the RHEED intensity is initially close to zero and then increases and eventually saturates.

Prior to GaN NW growth, the 7×7 surface reconstruction of the Si(111) substrate is observed and rapidly vanishes once the nitridation process begins by only opening the nitrogen shutter. The stage (I) of the nucleation phase starts with the subsequent opening of the gallium shutter (i.e., at $t = 0$ min). In this stage, no RHEED signal is detected, revealing the occurrence of an incubation period. A delay in the nucleation process owing to a massive gallium desorption at the high growth temperature of 780°C could be involved during this period as mentioned in Ref. 24. In particular, it has recently been reported from quadrupole mass spectrometry measurements that the gallium desorbing rate is fairly high in the very early stages of the self-induced growth of GaN NWs on a Si_xN_y amorphous interlayer.[21] Furthermore, since gallium adatoms adsorb and diffuse onto the surface, metastable 2D GaN nuclei are also expected to form during this period.[16,17]

The start of stage (II) takes place after an incubation time of 6.5 min and is marked by the occurrence of the first GaN spots along rings on the RHEED patterns as shown in the inset of Fig. 1. This stage is associated with the formation of the first stable 3D GaN nuclei. A typical HRTEM image of a GaN nucleus is shown in Fig. 2(a): spherical cap-shaped islands are nucleated on a continuous Si_xN_y amorphous interlayer with a thickness of 1.5 nm. Most likely, the preferential nucleation sites are surface defects like steps of the amorphous interlayer. The caps are further strongly spherical: Their free surface is composed of high-index atomic planes, which can be interpolated here by a curved surface. It is worth noticing that GaN thus nucleates, under strongly nitrogen-rich conditions and at high temperature, as spherical caps for the self-induced growth both on the AlN buffer layer and on the Si_xN_y amorphous interlayer.[16,17] Throughout the stage (II),

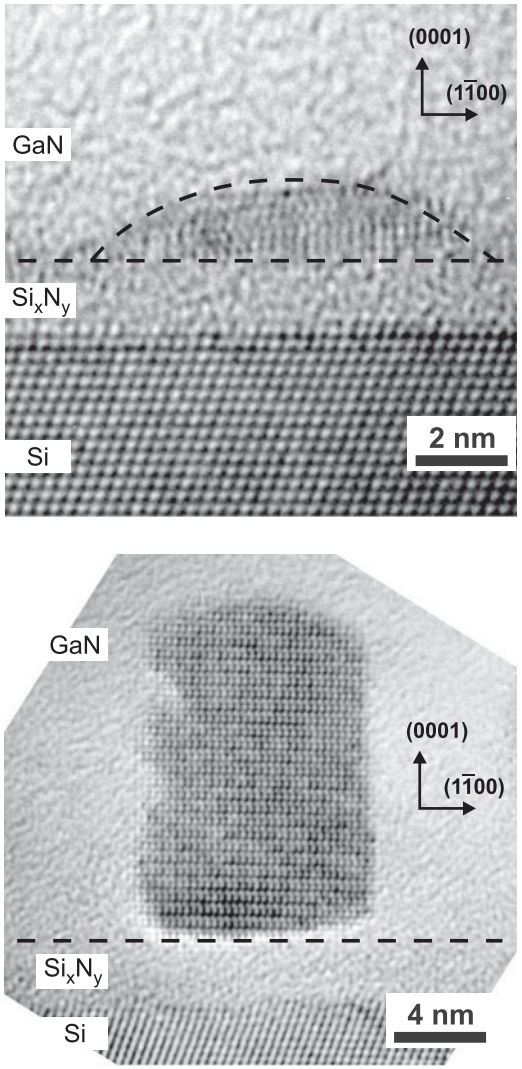

FIG. 2. HRTEM images collected on dedicated samples grown for 7 and 16 min, revealing the following respective GaN island shapes at the onset of the nucleation process: spherical cap-shaped island and NW. The NWs are hexahedral. The shape of spherical caps is outlined for the sake of clarity.

the spherical caps coarsen and their density increases, accounting for the rise of the RHEED intensity.

The start of stage (III) corresponds to the formation of the very first GaN NWs after a nucleation time of roughly 16 min and is deduced from HRTEM images collected on dedicated samples. An example of all the collected HRTEM images is presented in Fig. 2(b) and shows the presence of GaN NWs during this stage: NW-shaped islands having {0001} top facet and vertical sidewalls consistent with the presence of $\{1\,\bar{1}\,00\}$ planes (i.e., *m*-planes) are observed. The GaN NWs are expected to be gallium-polar as reported in Ref. 11. GaN islands thus undergo a shape transition from spherical caps to NWs during stage (III). It should be noted here that no pyramid-shaped islands are detected in contrast to the self-induced growth on the AlN buffer layer,[16,17] showing that faceting does not proceed. This remarkable difference in the nucleation process is attributed to the distinct features of the strain: On the AlN buffer layer, the shape transition toward pyramid-shaped islands enable the elastic relaxation of the epitaxial strain in the initial spherical caps. In comparison, on the Si_xN_y amorphous interlayer, the epitaxial constraint is much weaker and the epitaxial strain is therefore very low.

Eventually, the stage (IV) starts with the constancy of the RHEED intensity after a growth time of 20 min: This constancy could be attributed to the saturation of the overall spherical cap and NW density. It should be noted that the presence of spherical caps is still detected in this stage, suggesting that the shape transition between spherical caps and NWs statistically takes place at different growth durations. It is expected that the NW density continuously increases with respect to the spherical cap density for longer growth durations.

B. The role of surface stress, surface free energy, and edge effects in the shape transition towards the NW morphology

1. Direct evidence of the shape transition

The height h and radius r_0 of spherical caps and NWs are systematically determined from HRTEM images recorded on dedicated samples in the stages (II), (III), and (IV), as shown in Fig. 3. There exist two separate ranges of specific sizes for spherical caps and NWs. The spherical caps have a typical radius and height systematically smaller than 5 and 2 nm, respectively. Their wetting angle θ further equals $42\pm7^\circ$ in the entire range of their sizes and hence is smaller than 90°, as shown by the straight lines in Fig. 3 delineating the experimental data points: This indicates that GaN wets the Si_xN_y amorphous interlayer and that the spherical caps coarsen with a given wetting angle, namely by retaining their shape. The shape transition from spherical caps toward the NW morphology is therefore discontinuous and of first-order type. The formation of the very first GaN NWs abruptly occurs at an experimental critical radius of 5 nm, which is liable to be highly dependent on the growth conditions as discussed later.

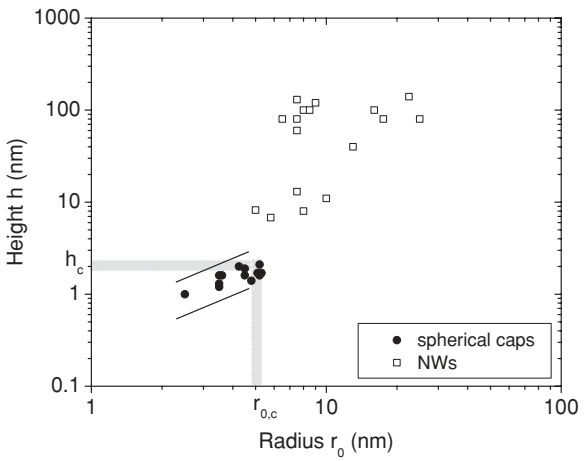

FIG. 3. Height h as a function of radius $r_0$obtained from HRTEM images for the two different shapes of GaN islands as growth proceeds: the spherical caps and NWs are observed on dedicated samples grown for 7, 11, 16, and 24 min and 16 and 24 min, respectively. The gray color regions correspond to the experimental critical height and radius of NWs.

From geometrical considerations, a critical height of about 2 nm is also determined.

In order to account for the shape transitions in quantum dot and NW growth, several thermodynamic approaches have been developed and indicate that the preferential island shape minimizes its total free energy per unit volume. As can be seen in the review of Shchukin and Bimberg,[25] the total free energy per unit volume of a three-dimensional island is given by the following relation:

$$E_{\text{tot}} = E_{\text{strain}} + E_{\text{interface}} + E_{\text{surface}} + E_{\text{edge}}, \tag{1}$$

where $E_{\text{strain}}, E_{\text{interface}}, E_{\text{surface}}$, and E_{edge} are the respective strain, interface, surface, and edge energy per unit volume. In the following, we focus on each contribution to the total free energy so as to identify the predominant driving force leading to the shape transition towards the NW morphology.

2. *The strain energy: the effects of surface stress as a strain source*

The strain energy generally originates from the strain induced by the lattice mismatch with the substrate. However, as the epitaxial constraint is very weak for the self-induced growth on the Si_xN_y amorphous interlayer, no significant epitaxial strain is expected here within the islands in contrast to the self-induced growth on the AlN buffer layer.[16,17] Instead, we point out that another strain source usually less intense is predominant due to the very small dimensions of spherical caps and NWs. It is discussed here whether this strain source plays a significant role in the nucleation mechanisms. In three-dimensional islands, the lattice parameter close to the surface slightly differs from the lattice parameter in the bulk, leading to the existence of a force per unit length typically called surface stress f. Such a surface stress can be considered as exerting an equivalent Laplace pressure P on the island surfaces, which is given by:

$$P = f\frac{dA}{dV}, \tag{2}$$

where A and V are the island surface area and volume, respectively.[22,26,27] The Laplace pressure $P_{\text{spherical-caps}}$ acting on the free surface of spherical caps equals:

$$P_{\text{spherical-cap}} = \frac{2a(\theta)\, f}{r_0}, \tag{3}$$

where $a(\theta) = [\sin^3\theta/(2 - 3\cos\theta + \cos^3\theta)] + [2(1 - \cos\theta)\sin\theta/(2 - 3\cos\theta + \cos^3\theta)]$ is a numerical constant calculated for a wetting angle of 42°. This Laplace pressure is dependent only on the radius. In contrast, the Laplace pressures $P_{\text{NW-top-facet}}$ and $P_{\text{NW-sidewalls}}$ acting on the NW top facet and vertical sidewalls, respectively, are given by:

$$P_{\text{NW-top-facet}} = \frac{4f}{\sqrt{3}r_0} \tag{4}$$

$$P_{\text{NW-sidewalls}} = \frac{2f}{h} + \frac{2f}{\sqrt{3}r_0}. \tag{5}$$

While $P_{\text{NW-top-facet}}$ only depends on the radius, $P_{\text{NW-sidewalls}}$ is dependent on both the height and radius. It should be noted here that the surface stress is by definition a tensor, which is taken here in a first approximation as isotropic and equals

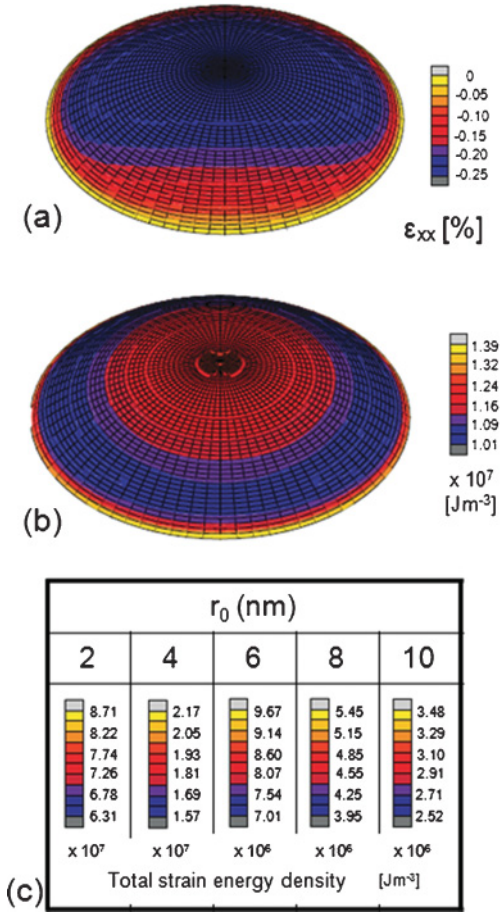

FIG. 4. (Color online) Spatial distribution of (a) the Laplace-pressure-induced strain (ε_{xx} component) and of (b) the strain energy density for a spherical-cap-shaped island with a radius of 5 nm. The legend in (c) shows the reduction of the total strain energy density with increasing the radius.

1.9 N/m in GaN.[28] As the Laplace pressure within spherical caps and NWs inversely scales with their sizes, its magnitude is significant and of the order of several GPa in the nanoscale dimensions. The Laplace pressure thus leads to the generation of strong volume elastic strain within the islands, which is quantitatively and spatially determined by FEM calculations:[22] The Laplace pressure is considered as acting perpendicular to each surface element while the GaN-silicon nitride interface has to obey a fixed mechanical boundary condition.

The spatial distribution of the Laplace-pressure-induced strain and of the related strain energy density E_{strain} is presented in Figs. 4 and 5 for spherical caps and NWs, respectively, with the same volume and the same radius of 5 nm. The mechanical constants are taken from Ref. 23: Their variation due to the nanoscale dimensions is neglected since both spherical caps and NWs have very close sizes.[29] It is clearly revealed that the spatial distribution is uniform neither within the spherical caps nor within the NWs. The Laplace-pressure-induced strain (i.e., the ε_{xx} component) is, for instance, at its maximum at the NW edges and at its minimum at the NW center as revealed in Fig. 5(a).

The strain energy density is also highly concentrated at the NW edges and especially at the corners but is much smaller

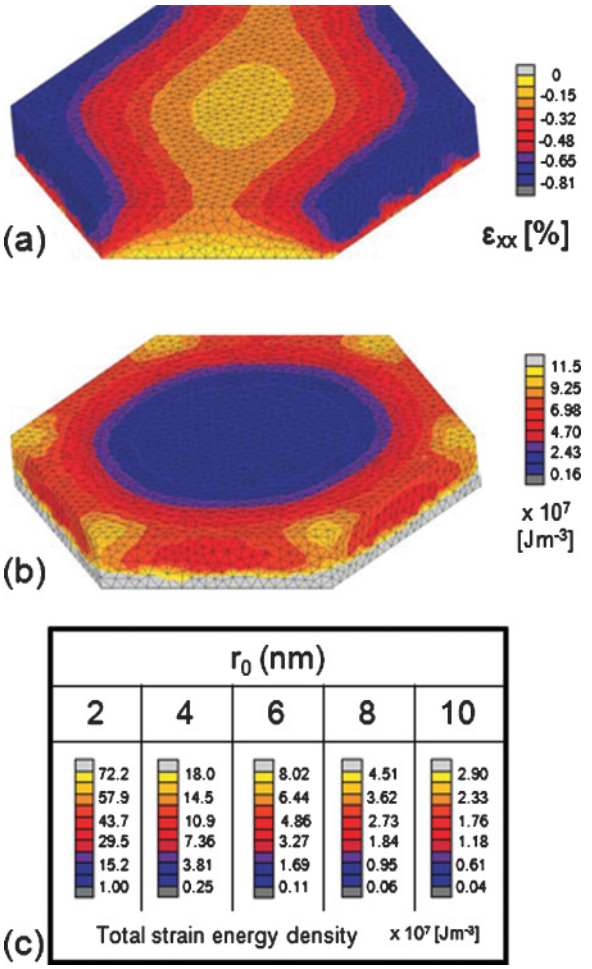

FIG. 5. (Color online) Spatial distribution of (a) the Laplace-pressure-induced strain (ε_{xx} component) and of (b) the total strain energy density for a NW with a radius of 5 nm. The legend in (c) shows the reduction of the total strain energy density with increasing the radius.

by a factor of about 70 in the center, as seen in Fig. 5(b). This reveals that the NW geometry is very efficient in relieving the Laplace-pressure-induced strain. In contrast, the strain energy density in spherical caps is only slightly stronger by a factor of about 1.4 at the edges than at the center, as shown in Fig. 4(b). The NW geometry yields the smallest and highest local strain energy density values. Nevertheless, we point out that the highest strain energy density is strongly localized close to the NW surface and rapidly decreases toward the bulk. As a consequence, the strain energy density due to the Laplace pressure is on average smaller in the NW geometry than in spherical caps for a given volume and radius. Figures 4(c) and 5(c) display legends for different radii. The same relations discussed above for a radius of 5 nm hold valid also for all other considered island sizes. Thus, the NW geometry is liable to support a larger surface stress than spherical caps, which further induces a lower strain energy density: In other words, the NW geometry is more efficient than the spherical cap shape in accommodating the effects of surface stress. It should be noted that this finding is in agreement with the literature: For instance, it is theoretically predicted and experimentally

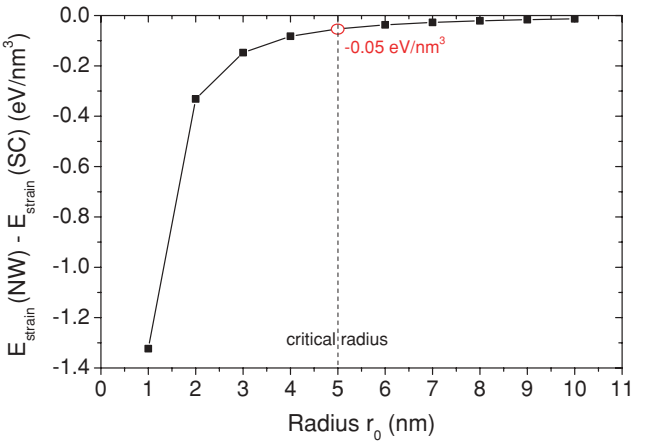

FIG. 6. (Color online) Evolution of the driving force related to strain energy as a function of the island radius. This driving force is defined as the difference between the smallest total strain energy density from FEM calculations of spherical caps with a wetting angle of 42° and of NWs for a given radius.

observed that the NW geometry can undergo plastic relaxation for larger sizes, namely storing a higher elastic strain energy, as compared to three-dimensional islands with less steeply inclined sidewalls and the same volume.[16,30–32]

As a consequence, the difference $E_{\text{strain}}(\text{NW}) - E_{\text{strain}}(\text{SC})$ is expected to be negative and can be considered as a driving force in favor of the shape transition. Numerical values have been calculated on the basis of the data presented above and are plotted in Fig. 6 for various radii. Interestingly, the magnitude of this driving force depends on the sizes of both spherical caps and NWs. The driving force is lower and lower with increasing the radius for a given volume: The driving force is reduced by two orders of magnitude when the radius increases from 1 to 10 nm. Indeed, the Laplace pressure is continuously reduced when the islands coarsen owing to the reduction of the surface-to-volume ratio. The coarsening process of spherical caps thus leads to the relief of the Laplace-pressure-induced strain by decreasing the magnitude of the Laplace pressure itself. At the same time, the related driving force in favor of the shape transition is also reduced.

3. *The interface and surface energy: its anisotropy as the predominant driving force*

As can be seen in Eq. (1), deduced from the review of Shchukin and Bimberg,[25] it is necessary to take into account other contributions to the total free energy such as the surface and interface energy besides the strain energy. As the shape transition occurs at a given radius, the interface area does not change and hence the interface energy does not play a significant role. The free surface of spherical caps has a surface energy γ_{SC} roughly given by $(\gamma_{\text{SiN}} - \gamma_i)/\cos\theta$ according to the Young equation, where γ_{SiN} and γ_i are the amorphous Si_xN_y surface energy and interface energy, respectively. Giving a value for the interface energy γ_i between the GaN spherical cap and the Si_xN_y amorphous interlayer is here not straightforward due to the lack of data in the literature. Nevertheless, the interface energy between a crystalline and an amorphous material is commonly fairly low. As a matter

of fact, the interface energy between crystalline silicon and amorphous silicon dioxide, for instance, is only several tens of millielectron volts per square angstrom.[33] Accordingly, the interface energy is chosen here as smaller than 40 meV/Å^2 as a first approximation: This numerical value is expected to be the upper limit. A rough upper estimate of the free surface energy γ_{SC} of spherical caps is thus about 176 meV/Å^2 by taking $\gamma_{SiN} = 171$ meV/Å^2 [i.e., for crystalline $Si_3N_4(0001)$ layer], $\gamma_i = 40$ meV/Å^2 and $\theta = 42°$.[33,34] Nevertheless, it should be noted that the silicon surface energy is much higher in its crystalline variant (i.e., 1.36 J/m^2) than in its amorphous variant (i.e., 1.09 J/m^2) and is hence reduced by a factor of 1.25, which may be similar in a first approximation for the amorphous Si_xN_y surface energy.[35,36] Accordingly, a rough lower estimate of the free surface energy γ_{SC} of spherical caps is about 130 meV/Å^2 by taking $\gamma_{SiN} = 137$ meV/Å^2 (i.e., extrapolated for amorphous Si_3N_4 layer), $\gamma_i = 40$ meV/Å^2 and $\theta = 42°$.[33,34] We point out that the surface energy has been determined with the upper expected value of the interface energy and does not consider surface reconstructions.

In contrast, the NW top facet and vertical sidewalls are composed of *c*- and *m*-planes, respectively, which have as close-packed planes in the wurtzite structure by definition a very low surface energy. The *m*-plane surface energy $\gamma_{m\text{-plane}}$ equals 118 meV/Å^2 as given in Ref. 37. The *c*-plane surface energy $\gamma_{c\text{-plane}}$ is expected to be lower according to the broken-bond model,[38] for instance, despite the lack of data in the literature and about 110 meV/Å^2 in correlation with the (111) plane surface energy that is the lowest one in the zinc blende structure. In comparison, the free surface energy in spherical caps is hence much higher, since the surface is composed of high-index planes. However, the free surface areas of NWs and of spherical caps are given by $S_{area}(NW) = 6r_0h + (3\sqrt{3}/2)r_0^2$ and $S_{area}(SC) = [2\pi(1-\cos\theta)/\sin^2\theta)]r_0^2$, respectively. It should be noted that thus the free surface area is larger in NWs than in spherical caps, as shown in Fig. 7. In other words, the increase in the free surface area by changing the island shape from spherical caps to NWs is not in favor of the transition if the difference in surface free energy per unit area is not taken into account. Eventually, the total free surface energy of NWs and spherical caps, respectively denoted as $E_{surface}(SC)$ and $E_{surface}(NW)$, are given by:

$$E_{surface}(SC) = 2\pi\left(\frac{1-\cos\theta}{\sin^2\theta}\right)r_0^2\gamma_{SC} \quad (6)$$

$$E_{surface}(NW) = 6r_0h\gamma_{c\text{-plane}} + \frac{3\sqrt{3}}{2}r_0^2\gamma_{m\text{-plane}}. \quad (7)$$

It is clearly revealed in Fig. 7 that the total free surface energy per unit volume is smaller in NWs than in spherical caps, showing that the anisotropy of surface energy that is in favor of the NW morphology is stronger than the increase in their free surface area that is against the NW morphology. As a consequence, the anisotropy of surface energy acts as a driving force for the shape transition toward the NW morphology. The magnitude of this driving force continuously decreases by one order of magnitude when the radius rises from 1 to 10 nm as shown in Fig. 7. This decrease is due to the reduction of the surface over volume ratio, similarly to the situation for

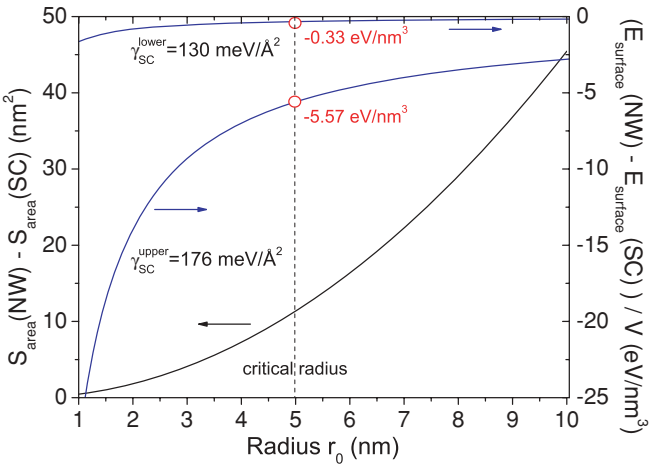

FIG. 7. (Color online) Evolution of (a) surface areas S_{area} and of (b) the driving force related to surface energy as a function of the island radius r_0. This driving force is defined as the difference between the total free surface energy from Eqs. (5) and (6) per unit volume of spherical caps with a wetting angle of 42° and of NWs for a given radius. The plot is given for the lower and upper values of spherical cap surface energy γ_{SC}.

the Laplace-pressure-induced strain. More importantly, the comparison of Figs. 6 and 7 yields that the driving force corresponding to the anisotropy of surface energy is much stronger than the one due to strain energy density induced by the Laplace pressure. It is thus deduced that the shape transition from the spherical caps toward the NW morphology is predominantly governed by the anisotropy of surface energy. It is worth noticing here that considering a higher surface energy in spherical caps than in NWs may also lead to a higher surface stress in correlation with the Shuttleworth equation.[39] Nevertheless, increasing the surface stress in spherical caps inevitably results in the increase in the strain energy density as compared to the NW geometry, which still favors the shape transition.

4. The edge energy as an energy barrier

From our previous theoretical results, both the strain energy related to the effects of surface stress and the surface energy are on average smaller in the NW geometry than in spherical caps and hence act as a driving force for the shape transition. It was found that the magnitude of the driving force related to surface energy is much stronger than the magnitude of the driving force related to strain energy, showing that the anisotropy of surface energy is the predominant driving force for the shape transition. In principle, the NW morphology is thus energetically favorable with respect to the spherical cap shape from the contributions of the strain and surface energy to the total free energy.

It should be, however, noted here that the evolution of both the strain energy density and the surface energy per unit volume is continuous with increasing the radius, which would suggest a continuous shape transition from spherical caps toward the NW morphology. In contrast, it has experimentally been found out previously that spherical caps coarsen with

retaining their shape until reaching an experimental critical radius of 5 nm, showing that the shape transition is instead of first-order type (i.e., discontinuous). In order to agree both the experimental and theoretical results, it is inferred that an energy barrier does exist and has to be overcome to favor the shape transition. This points out that another contribution to the total free energy as given in Eq. (1) plays a crucial role in favor of the spherical cap shape. This contribution is expected to be especially predominant for the very small radii lower than 5 nm, for which the spherical cap shape is energetically favorable. It is proposed here that edge effects such as edge energy for instance must be involved at the very small nanoscale dimensions: Indeed, for radii lower than 5 nm, the ratio of the typical dimension of edges over the radius is fairly high, showing that edge effects can be dominant.[25,40] It has already been reported that the edge energy can have a strong influence on the formation energy of germanium island and lead to the presence of a maximum despite the continuous evolution of the surface and strain energy.[41] In addition, the edges of spherical caps and NWs have strongly different geometries and structural properties. For instance, the edge area is much larger in NWs than in spherical caps due to the presence of vertical sidewalls. Similarly, the NW edges are composed of corners, which are expected to retain a very high edge energy. This may lead to a higher total edge energy in NWs than in spherical caps, accounting for the energy barrier to be overcome in order to favor the shape transition. One indication in that sense is given in Figs. 4 and 5: the strain energy density related to surface stress is larger at the NW edges and corners than at the spherical cap edges. We stress that such an energy barrier is reduced with increasing the radius. As the driving force corresponding to the strain and surface energy also decreases with increasing the radius, it is expected that edge effects lessen more quickly, which can reveal a discontinuous shape transition. Eventually, it should be further noted that island coarsening is the key growth process as it reduces edge effects and can account for the occurrence of a critical radius once the energy balance becomes in favor of the NW morphology.

5. *The effects of the growth conditions*

We emphasize that the growth conditions also have an influence on the value of the critical radius, as the surface energy highly depends on the surface reconstructions at work and thus on the V/III ratio. This may in particular change the wetting behavior of the spherical caps on the Si_xN_y amorphous interlayer and thus the energy balance between the strain energy induced by the Laplace pressure, the surface free energy, and edge effects. This reveals that the critical radius is expected to be strongly dependent on the growth conditions, accounting for the smaller critical radius found by Stoica *et al.*, for instance.[19]

IV. CONCLUSION

We have investigated the nucleation mechanisms of self-induced GaN NWs grown by plasma-assisted MBE on a Si_xN_y amorphous interlayer by combining *in situ* RHEED measurements with HRTEM imaging. From our experimental results, it is clearly shown that GaN does not nucleate in the NW shape but initially as spherical-cap-shaped islands with a wetting angle of $42 \pm 7^\circ$. Subsequently, these spherical caps coarsen while retaining their shape and eventually undergo a shape transition toward the NW morphology at an experimental critical radius of 5 nm. In contrast to the self-induced growth on the AlN buffer layer, no pyramid-shaped islands are formed, showing that the epitaxial constraint is very weak. From our theoretical results, it is clearly revealed that the Laplace pressure related to the effects of surface stress induces significant volume elastic strain in both spherical caps and NWs. This effect is in this case the predominant strain contribution owing to the very low epitaxial strain. The NW geometry is liable to more efficiently relieve the Laplace-pressure-induced strain as inferred from analytical and FEM calculations. The strain energy density is on average smaller in the NW geometry than in spherical caps and acts therefore as a driving force for the shape transition. Simultaneously, the anisotropy of surface energy is also found to be in favor of the shape transition towards the NW morphology. This is due to the presence of *c*- and *m*-planes with very low surface energies in NWs as compared to the free surface composed of high-index planes in spherical caps. It is further demonstrated that the anisotropy of surface energy is the predominant driving force compared to the difference in strain energy. It is also deduced from thermodynamic considerations that an energy barrier has to be overcome to favor the shape transition and is highly efficient for very low radii below 5 nm: This energy barrier may be related to edge effects. The shape transition leading to the self-induced formation of the very first GaN NWs occurs at the critical radius at which the anisotropy of surface energy is stronger than edge effects.

ACKNOWLEDGMENTS

This work was partly supported by the German BMBF joint research project MONALISA (Contract no. 01BL0810) and the European Community within the FP7 project SMASH (Contract no. 228999). One of the authors (M.K.) acknowledges financial support by the German National Academic Foundation.

*Current address: Laboratoire des Technologies de la Microélectronique, CNRS-UJF-Grenoble INP, 17 rue des Martyrs, F-38054 Grenoble, France.

[1] M. Law, J. Goldberger, and P. Yang, Annu. Rev. Mater. Res. **34**, 83 (2004).

[2] C. M. Lieber and Z. L. Wang, MRS Bull. **32**, 99 (2007).

[3] R. S. Wagner and W. C. Ellis, Appl. Phys. Lett. **4**, 89 (1964).

[4] B. A. Wacaser, K. A. Dick, J. Johansson, M. T. Borgström, K. Deppert, and L. Samuelson, Adv. Mater. **21**, 153 (2009).

[5] X. F. Duan, J. F. Wang, and C. M. Lieber, Appl. Phys. Lett. **76**, 1116 (2000).

[6] M. T. Bjork, B. J. Ohlsson, T. Sass, A. I. Persson, C. Thelander, M. H. Magnusson, K. Deppert, L. R. Wallenberg, and L. Samuelson, Appl. Phys. Lett. **80**, 1058 (2002).

[7]M. Yoshizawa, A. Kikuchi, M. Mori, N. Fujita, and K. Kishino, Jpn. J. Appl. Phys. **36**, L459 (1997).
[8]M. A. Sanchez-Garcia, E. Calleja, E. Monroy, F. J. Sanchez, F. Calle, E. Muñoz, and R. Beresford, J. Cryst. Growth **183**, 23 (1998).
[9]W. I. Park, D. H. Kim, S. W. Jung, and G. C. Yi, Appl. Phys. Lett. **80**, 4232 (2002).
[10]J. J. Wu and S. C. Liu, J. Phys. Chem. B **106**, 9546 (2002).
[11]C. Chèze, L. Geelhaar, O. Brandt, W. Weber, H. Riechert, S. Münch, R. Rothemund, S. Reitzenstein, A. Forchel, T. Kehagias, P. Komninou, G. P. Dimitrakopulos, and T. Karakostas, Nano Res. **3**, 528 (2010).
[12]R. K. Debnath, R. Meijers, T. Richter, T. Stoica, R. Calarco, and H. Lüth, Appl. Phys. Lett. **90**, 123117 (2007).
[13]K. A. Bertness, A. Roshko, L.M. Mansfield, T. E. Harvey, and N. A. Sanford, J. Cryst. Growth **310**, 3154 (2008).
[14]J. Ristíc, E. Calleja, S. Fernández-Garrido, L. Cerutti, A. Trampert, U. Jahn, and K. H. Ploog, J. Cryst. Growth **310**, 4035 (2008).
[15]R. Calarco, R. Meijers, R. K. Debnath, T. Stoica, E. Sutter, and H. Lüth, Nano Lett. **7**, 2248 (2007).
[16]V. Consonni, M. Knelangen, L. Geelhaar, A. Trampert, and H. Riechert, Phys. Rev. B **81**, 085310 (2010).
[17]M. Knelangen, V. Consonni, A. Trampert, and H. Riechert, Nanotec. **21**, 245705 (2010).
[18]O. Landré, C. Bougerol, H. Renevier, and B. Daudin, Nanotec. **20**, 415602 (2009).
[19]T. Stoica, E. Sutter, R. J. Meijers, R. K. Debnath, R. Calarco, H. Lüth, and D. Grützmacher, Small **4**, 751 (2008).
[20]F. Furtmayr, M. Vielemeyer, M. Stutzmann, J. Arbiol, S. Estradé, F. Peirò, J. R. Morante, and M. Eickhoff, J. Appl. Phys. **104**, 034309 (2008).
[21]C. Chèze, L. Geelhaar, A. Trampert, and H. Riechert, Appl. Phys. Lett. **97**, 043101 (2010).
[22]R. C. Cammarata, T. M. Trimble, and D. J. Srolovitz, J. Mater. Res. **15**, 2468 (2000).
[23]A. Polian, M. Grimsditch, and I. Grzegory, J. Appl. Phys. **79**, 3343 (1996).
[24]G. Koblmüller, P. Pongratz, R. Averbeck, and H. Riechert, Appl. Phys. Lett. **80**, 2281 (2002).
[25]V. A. Shchukin and D. Bimberg, Rev. Mod. Phys. **71**, 1125 (1999).
[26]R. C. Cammarata, Prog. Surf. Sci. **46**, 1 (1994).
[27]H. Ibach, Surf. Sci. Rep. **29**, 195 (1997).
[28]A. Krost, A. Dadgar, J. Bläsing, A. Diez, T. Hempel, S. Petzold, J. Christen, and R. Clos, Appl. Phys. Lett. **85**, 3441 (2004).
[29]C. Q. Chen, Y. Shi, Y. S. Zhang, J. Zhu, and Y. J. Yan, Phys. Rev. Lett. **96**, 075505 (2006).
[30]F. Glas, Phys. Rev. B **74**, 121302(R) (2006).
[31]K. L. Kavanagh, Semicond. Sci. Technol. **25**, 024006 (2010).
[32]H. Ye, P. Lu, Z. Yu, Y. Song, D. Wang, and S. Wang, Nano Lett. **9**, 1921 (2009).
[33]Y. Tu and J. Tersoff, Phys. Rev. Lett. **84**, 4393 (2000).
[34]J. C. Idrobo, H. Iddir, S. Ögüt, A. Ziegler, N. D. Browning, and R. O. Ritchie, Phys. Rev. B **72**, 241301(R) (2005).
[35]D. J. Eaglesham, A. E. White, L. C. Feldman, N. Moriya, and D. C. Jacobson, Phys. Rev. Lett. **70**, 1643 (1993).
[36]S. Hara, S. Izumi, T. Kumagai, and S. Sakai, Surf. Sci. **585**, 17 (2005).
[37]J. E. Northrup and J. Neugebauer, Phys. Rev. B **53**, R10477 (1996).
[38]V. Jindal and F. Shahedipour-Sandvik, J. Appl. Phys. **106**, 083115 (2009).
[39]R. Shuttleworth, Proc. Phys. Soc. A **63**, 444 (1950).
[40]V. A. Shchukin, N. N. Ledentsov, P. S. Kop'ev, and D. Bimberg, Phys. Rev. Lett. **75**, 2968 (1995).
[41]O. E. Shklyaev, M. J. Beck, M. Asta, M. J. Miksis, and P. W. Voorhees, Phys. Rev. Lett. **94**, 176102 (2005).